





Article

Direct Mercury Detection in Landfill Leachate Using a Novel AuNP-Biopolymer Carbon Screen-Printed Electrode Sensor

Jae-Hoon Hwang ^{1,*}, David Fox ², Jordan Stanberry ³, Vasileios Anagnostopoulos ³, Lei Zhai ²
and Woo Hyoung Lee ^{1,*}

¹ Department of Civil, Environmental, and Construction Engineering, University of Central Florida, Orlando, FL 32816, USA

² NanoScience Technology Center and Department of Chemistry, University of Central Florida, Orlando, FL 32816, USA; foxd@knights.ucf.edu (D.F.); lzhai@ucf.edu (L.Z.)

³ Department of Chemistry, University of Central Florida, Orlando, FL 32816, USA; Stanberry.jordan@knights.ucf.edu (J.S.); Vasileios.Anagnos@ucf.edu (V.A.)

* Correspondence: Jaehoon.Hwang@ucf.edu (J.-H.H.); WooHyoung.Lee@ucf.edu (W.H.L.); Tel.: +14-07-823-5304 (W.H.L.)

Abstract: A novel Au nanoparticle (AuNP)-biopolymer coated carbon screen-printed electrode (SPE) sensor was developed through the co-electrodeposition of Au and chitosan for mercury (Hg) ion detection. This new sensor showed successful Hg²⁺ detection in landfill leachate using square wave anodic stripping voltammetry (SWASV) with an optimized condition: a deposition potential of −0.6 V, deposition time of 200 s, amplitude of 25 mV, frequency of 60 Hz, and square wave step voltage of 4 mV. A noticeable peak was observed at +0.58 V associated with the stripping current of the Hg ion. The sensor exhibited a good sensitivity of ~0.09 μA/μg (~0.02 μA/nM) and a linear response over the concentration range of 10 to 100 ppb (50–500 nM). The limit of detection (LOD) was 1.69 ppb, which is significantly lower than the safety limit defined by the United States Environmental Protection Agency (USEPA). The sensor had an excellent selective response to Hg²⁺ in landfill leachate against other interfering cations (e.g., Zn²⁺, Pb²⁺, Cd²⁺, and Cu²⁺). Fifteen successive measurements with a stable peak current and a lower relative standard deviation (RSD = 5.1%) were recorded continuously using the AuNP-biopolymer-coated carbon SPE sensor, which showed excellent stability, sensitivity and reproducibility and consistent performance in detecting the Hg²⁺ ion. It also exhibited a good reliability and performance in measuring heavy metals in landfill leachate.

Keywords: Au nanoparticle; biopolymer; co-electrode position; landfill leachate; square wave anodic stripping voltammetry (SWASV)



Citation: Hwang, J.-H.; Fox, D.; Stanberry, J.; Anagnostopoulos, V.; Zhai, L.; Lee, W.H. Direct Mercury Detection in Landfill Leachate Using a Novel AuNP-Biopolymer Carbon Screen-Printed Electrode Sensor. *Micromachines* **2021**, *12*, 649. <https://doi.org/10.3390/mi12060649>

Academic Editor: Eduardo Pinilla-Gil

Received: 5 May 2021

Accepted: 30 May 2021

Published: 1 June 2021

Publisher's Note: MDPI stays neutral with regard to jurisdictional claims in published maps and institutional affiliations.



Copyright: © 2021 by the authors. Licensee MDPI, Basel, Switzerland. This article is an open access article distributed under the terms and conditions of the Creative Commons Attribution (CC BY) license (<https://creativecommons.org/licenses/by/4.0/>).

1. Introduction

Mercury (Hg) pollution caused by industrial activity has been attracting global attention for decades [1–3]. Mercury occurs in many forms in aqueous solution depending on oxidation and reduction conditions [4]. The main forms of Hg exposure in the general population include methylmercury (MeHg) from seafood, inorganic mercury (I-Hg) from food, and mercury vapor (Hg⁰) from dental amalgam fillings [5]. Most Hg occurs in organic and inorganic forms of divalent mercury and Hg⁰, as a form of Hg dissolved in an aqueous phase [6]. Once Hg has reached surface waters or soils, microorganisms convert it to MeHg, a substance that can be absorbed quickly by most organisms including marine life. MeHg, upon consumption, can cause negative health effects (i.e., nerve, kidney and intestinal damage; stomach disruption; reproductive failure; and DNA alteration) [7]. Inorganic mercury, Hg⁰ and Hg²⁺, is released into the environment from a variety of anthropogenic and natural sources. In particular, Hg²⁺ ions are one of the largest hazardous Hg pollutants in aquatic ecosystems [8]. Furthermore, Hg²⁺ is not readily biodegradable and is prone

to bioaccumulation and biomagnification across trophic levels. Exposure to Hg^{2+} has been linked to several diseases; such as Minamata [9], acrodynia [10], cardiac [11] and neurological disorders, [12] and several developmental illnesses.

Surface water and groundwater are often polluted by untreated sewage water, industrial waste, gasoline, medical waste, electroplated steel and electronic parts. Since Hg accumulates in the ecosystem during tropospheric cycling, it is essential to regulate the presence of Hg^{2+} in drinking water and environmental systems. The United States Environmental Protection Agency (USEPA) has mandated an upper limit of 2 ppb (10 nM) of Hg^{2+} in drinking water [3], so monitoring of very low concentrations of Hg in the early stages of pollution is required to assess hidden risks. Various analytical methods such as atomic absorption spectrophotometry (AAS) [13], atomic fluorescence spectrometry (AFS) [14], inductively coupled plasma mass spectrometry (ICP-MS) [15], and X-ray fluorescence spectrometry [16] have been developed for detecting Hg. These are generally combined with cold vapor generation and amalgamation techniques to separate and pre-concentrate Hg to achieve a high sensitivity [17,18]. However, the complicated pretreatment requires a variety of different reagents and numerous preparation steps. Electrochemical techniques are very effective in detecting low concentrations of mercury because metal ions can be rapidly pre-concentrated on the electrode surface using methods such as anodic stripping voltammetry (ASV) [19]. In addition, modifying electrodes can offer ease of operation and low-cost and portable instrumentation [20]. The sensitivity and selectivity of Hg electrochemical sensors have been greatly improved by nanostructured electrodes, which provide a large surface area and intriguing properties [21–23].

Gold nanostructures have attracted great research interest in the voltammetric detection of mercury because of their high affinity [24], good catalytic ability [25], high adsorption capacities [26], and excellent mass transport [27,28]. Among the many methods to prepare AuNPs, the reduction of chloroauric acid (HAuCl_4) is the most popular [29], but recently, the use of polymers to synthesize AuNPs has been reported. For example, AuNPs were prepared in the presence of chitosan [21,22] and its derivative carboxymethylated chitosan [24]. Chitosan is recognized as a low-cost promising supplement to AuNPs and other metal film electrodes due to its relatively high mechanical strength, good adhesion to traditional electrochemical surfaces, high water permeability, biocompatibility and [30,31] ability to form stable chelates with transition metal ions [32]. However, the application of chitosan-coated AuNPs has been limited to specific applications due to their tendency to agglomerate and precipitate; therefore coupling with a suitable supporting substrate may increase their viability in preparation of metal composite sensors [33].

In this study, we demonstrated direct Hg^{2+} detection in real landfill leachate samples using a AuNP-biopolymer-coated carbon SPE sensor. AuNP and the biopolymer (chitosan) were coated onto a carbon SPE sensor by electrodeposition and gave enhanced sensing performance for Hg^{2+} detection through an increase in both electrochemical sensitivity and stability. Using the new sensor, systematic batch experiments were performed to determine the optimal deposition time amplitude and frequency for detecting Hg^{2+} ions using square wave anodic stripping voltammetry (SWASV). The sensor performance for the on-site monitoring of Hg^{2+} including calibration curves, potential interference, repeatability, recovery, and limit of detection (LOD) was then fully evaluated in a landfill leachate matrix. This study was the first to investigate direct electrochemical Hg^{2+} detection in a real wastewater sample.

2. Materials and Methods

2.1. AuNP-Chitosan Electrode Sensor Fabrication

AuNP-chitosan composite film was electrochemically deposited on a carbon screen-printed electrode (SPE) (RRPE1001C, Pine Research Instrumentation, Durham, NC, USA) as a working electrode. The nanocomposite solution contained chloroauric acid (HAuCl_4) and chitosan, based on the optimization ratio of chitosan to sensor performance used in a previous study [34]. The schematic illustration of the electrodeposition of the composite

material is presented in Figure S1. The AuNP and biopolymer nanocomposite was mixed at a 1:1 ratio (12 mg chitosan in 10 mL DI solution and 0.01 M HAuCl_4 solution), which was stirred for 24 h at 60 °C to achieve complete mixing. Then, 3 μL of the solution was dropped onto the surface of the carbon SPE sensor and completely deposited by electrodeposition at 6.4 mA/cm^2 DC for 1 h. The electrodeposition was repeated three times to achieve sufficient deposition of AuNPs. The fabricated sensor was cleaned with DI water, dried at room temperature, and stored under ambient conditions before use.

2.2. Structure Characterization of AuNP-Biopolymer Composite

The surface structures of the fabricated SPE sensors were obtained using an Ultra 55 scanning electron microscope (SEM) (ZEISS, Oberkochen, Germany). Elemental mapping of the surface was achieved through energy-dispersive X-ray spectroscopy (EDS) using a Noran System 7 EDS with a silicon drift X-ray detector (Thermo Scientific™, Waltham, MA, USA). To characterize the surface chemical and oxidation states, X-ray photoelectron spectroscopy (XPS) was performed by a Thermo Scientific ESCALAB Xi+ X-ray Photoelectron Spectrometer Microprobe (Thermo Scientific™, Waltham, MA, USA) with a twin-crystal, micro-focusing monochromator and an Al anode. The XPS analysis chamber during measurement was held at a pressure below 1.0×10^{-7} torr. Electrochemical impedance spectroscopy (EIS) spectra were measured using a PalmSens 3 EIS potentiostat (PalmSens Compact Electrochemical Interfaces, Houten, The Netherlands) under the three-electrode system in 10 mM potassium ferricyanide ($\text{K}_3\text{Fe}(\text{CN})_6$) solution at the frequency range 5 Hz to 50 kHz.

2.3. Chemicals and Sample Preparation

Analytical grade sodium acetate was obtained from Sigma-Aldrich (St. Louis, MO, USA) and used without further purification. To characterize the developed sensor for Hg detection, a 0.1 M acetate buffer solution (AcB) at pH 3.0 was used. We used a stock Hg solution (1 mg/mL in nitric acid, 7487-94-7, Sigma-Aldrich, St. Louis, MO, USA) ranging from 2 to 20 ppb in the electrolyte (i.e., acetate buffer). For the sensor evaluation in real wastewater, landfill leachate samples were obtained from a local landfill (Orange county landfill, Orlando, FL, USA). The characterization of the landfill leachate samples is shown in Table S1. Test water samples were prepared by spiking precalculated amounts of Hg^{2+} ranging from 10 to 100 ppb into the landfill leachate and the sensor performance of mercury detection was evaluated for various mercury concentrations. To adjust pH to 3, 0.1 M HCl was added to the landfill leachate sample. The samples were kept in room conditions of 23 °C with a relative humidity of 45%. The prepared Hg^{2+} test solutions were validated using a single quadrupole ICP-MS (iCAP-RQ, Thermo Scientific, Waltham, MA, USA).

2.4. Sensor Characterization and Electrochemical Mercury Detection

A 20 mL electrochemical cell (Compact Voltammetry Cell-Starter Kit, Pine Research Instrumentation, Durham, NC, USA) with an effective volume of 10 mL was used for Hg^{2+} detection, and each series was measured by a three-electrode system consisting of an AuNP-chitosan working electrode, carbon counter electrode (RRPE1001C, Pine Research Instrumentation, Durham, NC, USA), and Ag/AgCl reference electrode (MI-401, Microelectrodes, Inc., Bedford, NH, USA). We used a PalmSens 3 EIS (PalmSens Compact Electrochemical Interfaces, Houten, The Netherlands) as a potentiostat for all tests (Figure 1). Mercury detection using the developed AuNP-biopolymer SPE sensor was characterized using SWASV and CV. First, CV was performed at a scan rate of 50 mV/s in 0.1 M AcB (pH 3.0) with Hg^{2+} (50 ppb) to determine the potential window of the AuNP-biopolymer SPE sensor for Hg^{2+} detection and the potential where the Hg^{2+} stripping peak appears. For the Hg^{2+} measurement using SWASV, Hg^{2+} was electrochemically deposited on the working electrode at -0.8 V at pH 3.0 of 0.1 M AcB for 100 s, and the reduced Hg^{2+} was then stripped according to predetermined parameters (4 mV step potential, 25 mV amplitude, and 20 Hz frequency). For sequential measurements, the working electrode was

cleaned at +0.8 V for 60 s to remove remnants of Hg^{2+} ion before the next measurement. All tests were conducted in triplicate with a value of mean \pm standard deviation (SD). The LOD was calculated based on three times the signal-to-noise (S/N ratio of 3) using the Equation (1): $C_L = kS_B/b$ [35], where C_L signifies the detection limit, S_B represents the standard deviation of blank signals, k is a parameter with a value of 3, and b is the value of the calibration curve slope.

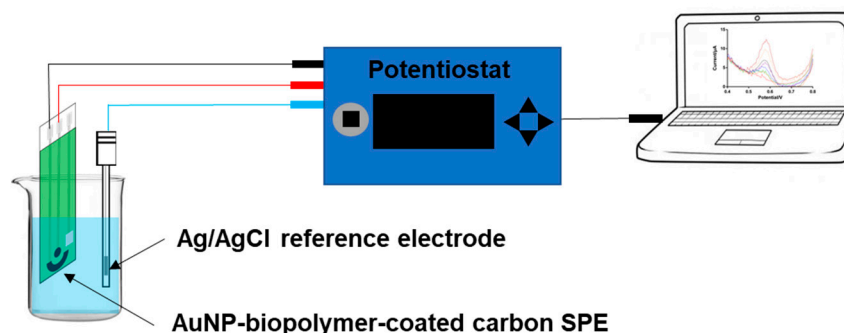


Figure 1. Measurement setup schematic for testing an AuNP-biopolymer-coated carbon SPE.

3. Results and Discussion

3.1. Characterization and Modification of AuNP-Biopolymer Nanostructure

The surface analysis by SEM showed that the electrode surface was covered with gold nano-urchins (AuNPs) as well as some small AuNPs, as seen in Figure 2. The AuNPs were on the order of 1 μm in diameter, with many spines on the surface of each urchin-like particle. The AuNPs shown on the electrode surface were in the tens of nanometers in diameter. Elemental analysis with energy-dispersive X-ray spectroscopy (EDS) mapping confirmed that the location of the Au signal was concentrated in these structures on the electrode surface. The EDS spectra (Figure S2) showed prominent characteristic X-ray peaks from C K_α and Au M emissions. In addition to the increased surface area, the Au urchin-like structures were expected to have improved performance through several mechanisms. For example, a greater portion of this exposed surface is likely composed of high-index facets. These have been shown to increase catalytic performance [36,37] and with Miller indices (hkl) (where at least one value is greater than 1) have a greater number of low-coordinated atoms on the surface [38]. These facets have higher surface energy, and as a result, the deposition takes place preferentially on these facets during particle growth. Co-electrodeposition of Au and chitosan successfully generated these urchin-like structures in addition to the free AuNPs on the surface of the SPE sensor.

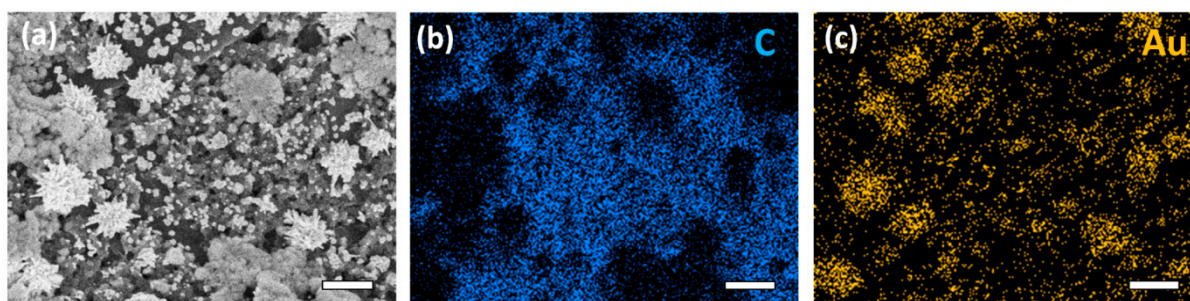


Figure 2. SEM and EDS mapping of AuNP-biopolymer composite film electrodeposited on a carbon electrode. The electron map obtained with the secondary detector is shown (a), with the corresponding carbon intensity map (b), and gold intensity map (c). All scale bars are 1 μm .

The surface chemical state was determined by XPS, as shown in Figure 3. Deconvolution of the C 1s and N 1s core-level peaks confirmed the surface adhesion of the biopolymer.

The C–C peak at 284.7 eV was the dominant peak in the sample, with a signal contribution from both the chitosan polymer and the exposed regions of the carbon electrode. Deconvolution analysis shows a C–N peak at 286.4 eV and a C–O peak at 287.2 eV, which are consistent with the structure of chitosan. The peak at 289.1 eV, consistent with C=O moiety, suggests some acetylated portions of the chitosan chain or residual carbon monoxide gas. Due to the low signal/noise ratio in the N 1s region, the deconvolution of the N 1s band is less certain; deconvolution may indicate an amide moiety peak at 400.0 eV, with $-\text{NH}_2$ and $-\text{NH}_3$ peaks at 399.3 eV and 400.7 eV, respectively, confirming a deacetylated chitosan biopolymer on the surface. Au 4f peaks were located at 84.5 eV ($4f_{7/2}$) and 88.3 eV ($4f_{5/2}$), with full width at half maxima (FWHM) of 0.80 eV and 0.76, respectively. The peak and FWHM are consistent with metallic Au [39].

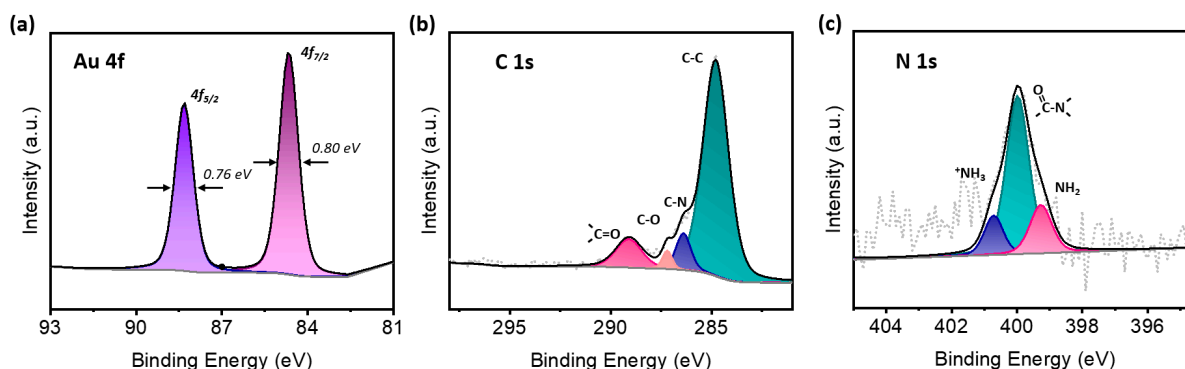


Figure 3. XPS of electrodeposited AuNP-biopolymer nanocomposite. (a) Au 4f spectra, (b) C 1s spectra, and (c) N 1s spectra.

3.2. AuNP-Biopolymer-Coated Carbon SPE Sensor Characterization

The electron transfer properties of the developed AuNP-biopolymer-coated carbon SPE sensor were studied by electrochemical impedance spectra (EIS) (Figure 4a). A carbon SPE sensor coated only with chitosan, one coated only with AuNPs, a bare carbon SPE sensor, and a bare gold SPE sensor were also prepared and compared for reference purposes. The charge transfer resistance for the chitosan-coated carbon SPE sensor (398 Ω) was higher compared to that of the bare carbon SPE sensor (228 Ω) and the bare gold SPE sensor (70 Ω), indicating that the chitosan only-coated carbon SPE sensor had hindered charge transfer from the redox probe of $[\text{Fe}(\text{CN})_6]^{3-/4-}$ to the surface of the fabricated electrode. In contrast, the Nyquist plots of the AuNP-coated SPE sensors (i.e., AuNP-coated carbon SPE sensor and AuNP-biopolymer-coated carbon SPE sensor) displayed an almost straight line, showing a very fast charge transport process due to direct electron transfer. This implied that the presence of AuNP nanocomposites enabled the enhancement of electron transfer kinetics suitable for achieving a superior sensor response. The value of the charge transfer resistance also depended on the dielectric properties at the electrode/electrolyte interface [40].

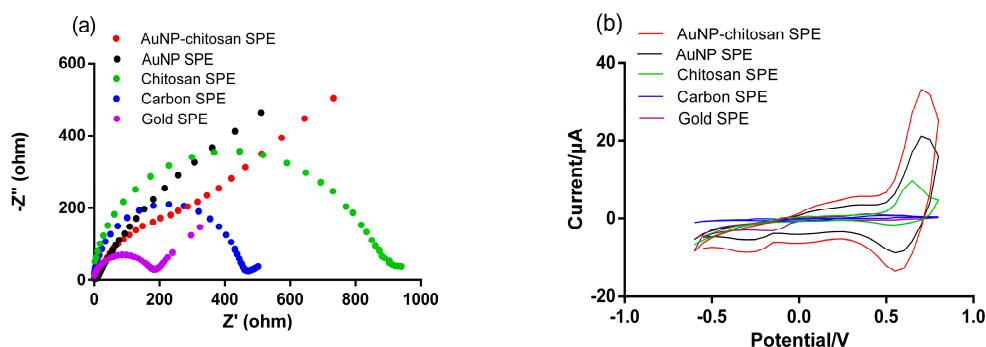


Figure 4. (a) Nyquist diagrams and (b) CV responses of a bare carbon SPE sensor, a bare gold SPE sensor, a biopolymer modified carbon SPE sensor, and an AuNP-biopolymer nanocomposite SPE sensor.

To investigate sensor characteristics for the oxidation and reduction of Hg^{2+} by varying potentials, CV was performed in 0.1 M AcB with a 50 ppb Hg^{2+} concentration (Figure 4b). The corresponding redox peaks current was gradually increased in the following order: chitosan-coated carbon SPE sensor, AuNP coated carbon SPE sensor, and AuNP-chitosan-coated carbon SPE sensor. The highest redox peak current was obtained with the AuNP-chitosan-coated carbon SPE sensor, which was attributed to the improvement in electron transport due to the metallic Au nanoparticles in chitosan. Lower redox peaks were observed for the bare electrode series (carbon and gold) due to the hindrance of electron transport because of the absence of the Au NP/chitosan composite on the working electrode. The observed findings were consistent with the results obtained from the EIS measurements. These results gave immediate evidence that the modification of the sensing interface successfully detected Hg^{2+} .

3.3. Optimization of SWASV Parameters for Hg^{2+} Detection

To achieve high performance in Hg^{2+} detection, the electrochemical parameters for SWASV (deposition potential, deposition time, amplitude, and frequency) were optimized at a fixed Hg^{2+} concentration of 20 ppb in 0.1 M AcB at pH 3.0. First, the effect of the deposition potential on Hg^{2+} -stripping peak currents was investigated between -1.0 and -0.2 V with a deposition time of 100 s, the amplitude of 25 mV and a frequency of 20 Hz [34] (Figure 5a). The current of 4.0 ± 0.1 μA at -0.6 V of deposition potential was 1.2–1.7 fold higher than other deposition potentials between -0.2 V and -1.0 V. The resulting SWASV peaks showed the maximum stripping peak current at -0.6 V, indicating the greatest reduction of Hg^{2+} . At deposition potentials higher than -0.6 V, the current obtained from stripping Hg^{2+} decreased as the deposition potential increased, probably due to the inefficient deposition of Hg^{2+} . On the other hand, at reduction potentials below -0.6 V, the reduction of Hg^{2+} was less efficient because the reaction began to compete with H_2 generation, which typically occurs below this potential [41,42]. As such, it could be seen that the stripping peak current decreased at a deposition potential lower than -0.6 V based on the CV tests. A similar trend of deposition potential was also obtained by Rahman et al. (2019) [43]. Thus, a deposition potential of -0.6 V was chosen as an optimum potential for Hg^{2+} .

Deposition time is known to affect the amount of Hg^{2+} ions [43] deposited on the AuNP-chitosan electrode, thus influencing the LOD and the overall time needed for the SWASV technique. The peak current of anodic Hg^{2+} stripping increased from 10.4 ± 0.6 to 39.7 ± 1.3 μA with a prolonged deposition time at the optimized deposition potential of -0.6 V (Figure 5b). The peak current for Hg^{2+} initially increased with deposition time, then slightly increased after 200 s probably due to Hg^{2+} saturation on the electrode surface. Although the sensitivity can be improved with a longer deposition time, surface saturation at high metal ion concentrations can also reduce the upper detection limit [44]. Correspondingly, the deposition time of 200 s was chosen as optimal for the fast detection of Hg^{2+} with high selectivity.

The effects of amplitude and frequency on the current response to Hg^{2+} were also investigated (Figure 5c,d). Optimal conditions for amplitude were observed at 25 mV with the highest peaks at 4.3 ± 0.04 μA . Increasing the amplitude range from 0.05 to 0.1 V resulted in higher ambient noise with a larger SD (Figure S3c) due to vibrations [45]. For frequency optimization, the peak heights increased from 20 to 100 Hz, while a higher frequency showed larger ambient noise after 80 Hz (Figure S3d) because of the frequency properties of vibration [45]. Therefore, 60 Hz was chosen as the optimal frequency for Hg^{2+} detection using the AuNP-chitosan SPE sensor. Overall, -0.6 V of deposition potential, 200 s of deposition time, 25 mV amplitude, and 60 Hz of frequency were selected as optimal SWASV analytical parameters for further evaluation of the sensor performance on Hg^{2+} detection.

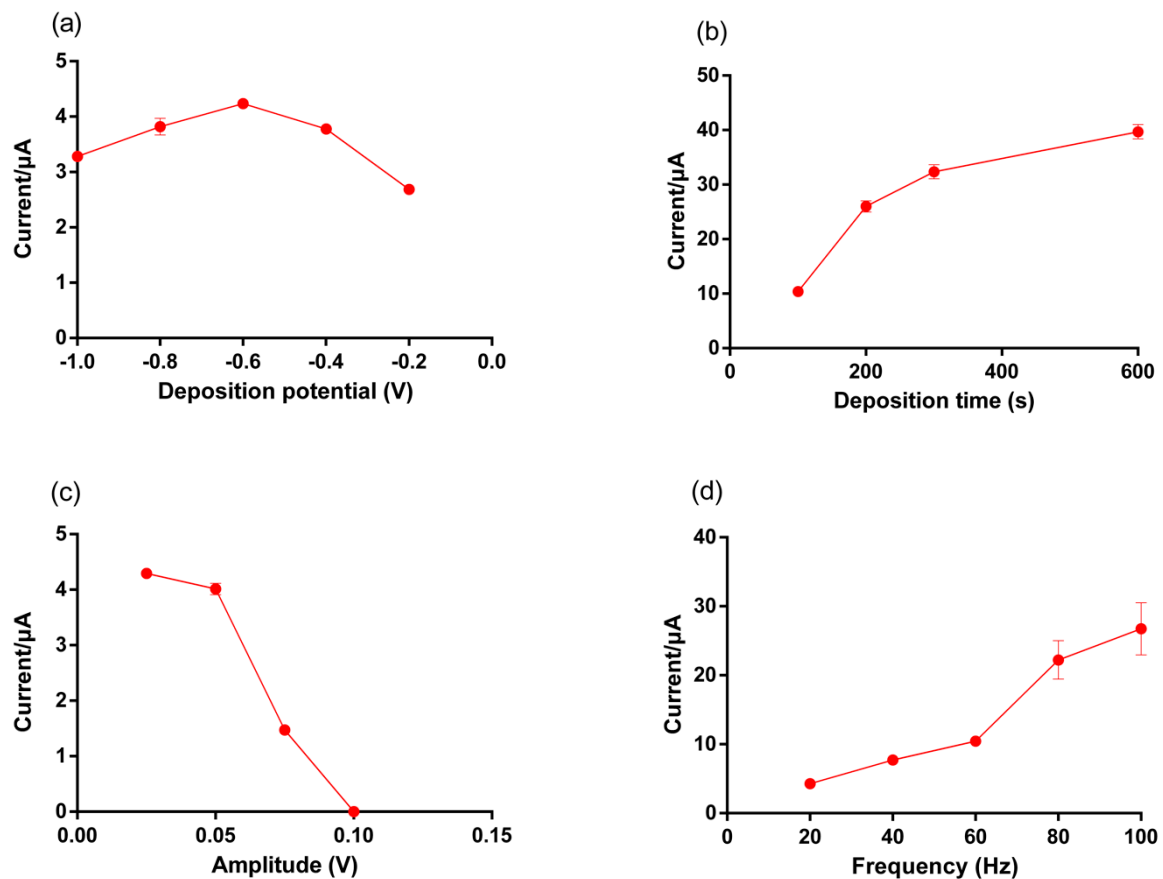


Figure 5. Optimization of (a) deposition potential, (b) deposition time, (c) amplitude and (d) frequency on the stripping peak currents of Hg^{2+} using an AuNP-biopolymer-coated SPE sensor. Hg^{2+} concentration was 10 ppb (0.1M AcB at pH 3.0). Individual data points represent the standard deviation ($\pm SD$) of duplicate experiments.

3.4. Sensitivity Analysis and Lifetime

Figure 6a shows the SWASV response of AuNP-biopolymer-coated carbon SPE sensor at various Hg^{2+} concentrations between 0–20 ppb in 0.1M AcB (pH 3.0) under optimized parameters. The well-defined sharp anodic stripping peaks for detecting Hg^{2+} were located at +0.58 V, and the peak currents were linearly increased with Hg^{2+} concentrations. The applied optimal parameter of the AuNP-biopolymer-coated carbon SPE sensor exhibited improved sensor sensitivity ($17\times$ more sensitive than an unoptimized one) with a higher R^2 value ($R^2 = 0.9914$), indicating enhanced sensitivity and stability for Hg^{2+} detection (Figure S4a,b). The correlation was $I_p = 0.477x + 0.0009$, where I_p is the stripping peak current (μA) and x is Hg^{2+} concentration (ppb) (Figure 6b). The sensitivity of the sensor was $\sim 0.1 \mu A/nM$ ($0.477 \mu A/\mu g$) according to the slope of the linear curve. The LOD of the AuNP-biopolymer-coated carbon SPE sensor toward Hg^{2+} was estimated to be 0.9 ppb according to Equation (1), which is well below the USEPA-defined limit for drinking water (2 ppb) [3]. The relative standard deviation (RSD) value of 2.27% was evaluated by replicate measurements ($n = 20$) of 20 ppb Hg^{2+} solution (Figure 6c). The linear range was also $25\times$ larger than that of other SPE sensors (bare gold and bare carbon) (Figure S4d,f). A comparison between the developed AuNP-biopolymer-coated carbon SPE sensor and other electrochemical Hg-detecting sensors, based on a gold electrode or AuNPs previously reported in the literature, is listed in Table 1. The AuNP-biopolymer-coated carbon SPE sensor had a lower Hg^{2+} detection range compared to those of previous studies. This is attributable to the AuNP surface, where free functional groups of amino acids (i.e., chitosan) exhibits a strong affinity for Hg^{2+} between Au and Hg [46]. The sensor also showed relatively lower RSD and detection limits.

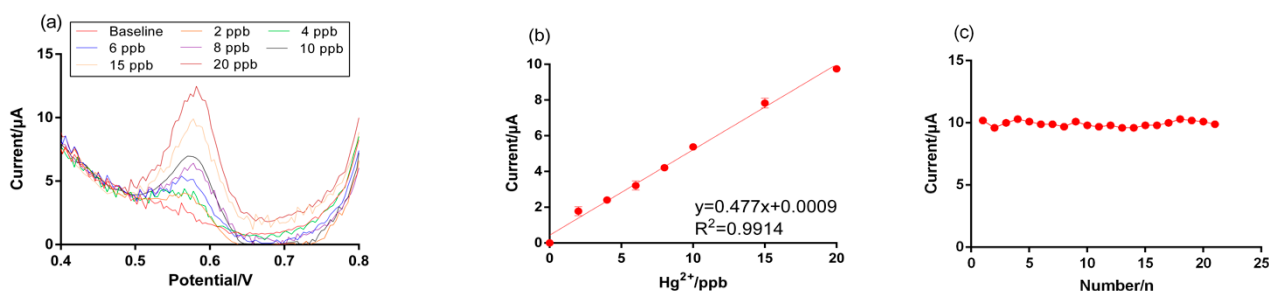


Figure 6. (a) SWASV replies for Hg^{2+} determination, (b) plot of the stripping peak current vs Hg^{2+} concentration, and (c) reproducibility. Deposition time is 200 s with a -0.6 V deposition potential, 0.004 V potential step, 0.025 V amplitude, and 60 Hz frequency. Hg^{2+} concentration was 20 ppb (0.1 M acetate buffer at pH 3.0). The error bars represent the standard deviation for the mean of the three replicate tests.

Table 1. Comparison of different types of sensor performance for electrochemical Hg (II) detection.

| Electrode | Method | Linear Range | LOD (nM) | RSD (%) | Reproducibility (n) | Sample Condition (Buffer Solution) | Reference |
|--|--------------------|----------------------|----------|---------|---------------------|------------------------------------|------------|
| AuNPs/CFME ⁽¹⁾ | DPASV ^a | 1–250 μM | 0.5 | 3.4 | — | 0.1 M HCl/pH 1 | [47] |
| np-AuNPs/ITO ⁽²⁾ | DPASV | 0.5–50 nM | 0.15 | 2.3 | 7 | 0.1 M HCl/pH 1 | [24] |
| Au-DMAET-(SWCNT-PABS) ⁽³⁾ | SWASV ^b | 20–250 μM | 63.4 | 2.7 | 10 | 0.1 M HCl/pH 3 | [48] |
| SWCNT-PhSH/Au ⁽⁴⁾ | SWASV | 5–90 nM | 3.0 | 3.8 | 7 | 0.1 M HCl/pH 1 | [49] |
| SPGE ⁽⁵⁾ | SWASV | 5–30 μM | 5.5 | 4.3 | 40 | 0.1 M HCl/pH 2 | [50] |
| AuNPs-GC ⁽⁶⁾ | CV ^c | 0.64–4 μM | 0.42 | — | — | 0.01 M HCl/pH 2 | [29] |
| Cys-AuNPs-CILE ⁽⁷⁾ | SWASV | 10–20,000 nM | 2.3 | 2.6 | 5 | 0.1 M phosphate/pH 7 | [51] |
| AuNP-biopolymer-coated carbon SPE sensor | SWASV | 10–100 nM | 4.5 | 2.3 | 20 | 0.1 M acetate/pH 3 | This study |

^a DPASV (differential pulse anodic stripping voltammetry); ^b SWASV (square wave anodic stripping voltammetry); ^c CV (cyclic voltammetry); ⁽¹⁾ Gold Nanoparticles (AuNPs)/three-dimensional fibril-like carbon-fiber mat electrode (CFME); ⁽²⁾ Nanoporous gold nanoparticles (np-AuNPs)/Indium tin oxide (ITO); ⁽³⁾ Au-dimethyl amino ethanethiol (DMAET)-Single-walled carbon nanotube-poly (m-amino benzene sulfonic acid) (SWCNT-PABS); ⁽⁴⁾ Single-walled carbon nanotube (SWCNTs) with thiophenol/Gold (Au); ⁽⁵⁾ Screen-printed gold electrodes (SPGE); ⁽⁶⁾ Gold nanoparticles-modified glassy carbon (AuNPs-GC); ⁽⁷⁾ l-cysteine (Cys)-Au nanoparticle-Carbon ionic liquid electrode (CILE).

3.5. Selectivity Analysis: Interference of Other Heavy Metals in Hg^{2+} Detection

Metal ions commonly found in water containing Hg^{2+} are known to compromise the accuracy of electrochemical measurements [48]. Thus, the influence of competing metal ions was investigated in two-fold concentrations over the analyte (i.e., 40 ppb) interfering species (Zn^{2+} , Cd^{2+} , Pb^{2+} , and Cu^{2+}) in 20 ppb Hg^{2+} in 0.1 M AcB (pH 3.0). Figure 7 shows a similar range of sensor responses in the presence of these heavy-metal ions. Most of these (Zn^{2+} , Cd^{2+} , and Pb^{2+}) did not interfere with the detection of Hg^{2+} . A slight decrease in the current value ($\sim 8.7\%$) was shown in the presence of Cu^{2+} , a major interfering species because of its close potential to Hg^{2+} measurement [52]. To further validate this, we performed an experiment by mixing ions with a fixed concentration of Hg^{2+} at 20 ppb. No decrease in peak current or interfering voltammetric peaks was observed in the solution. The developed AuNP-biopolymer-coated carbon SPE sensor was then applied to the Hg^{2+} detection in landfill leachate as an example of a practical analytical application.

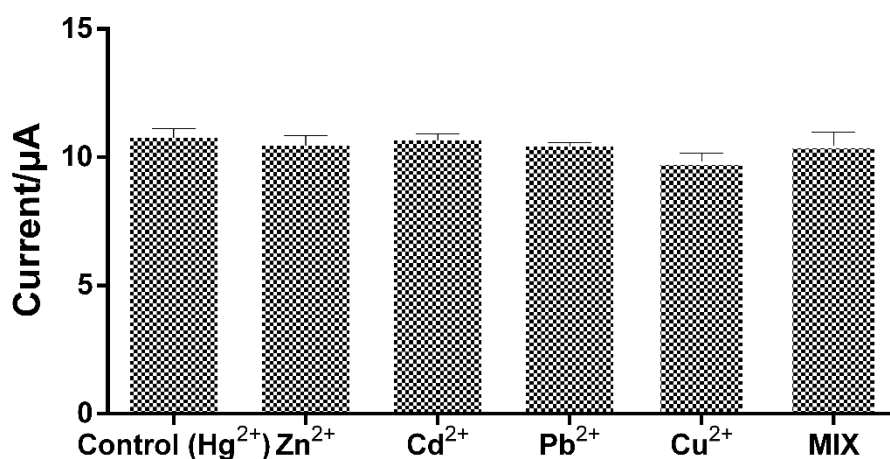


Figure 7. Sensor response changes at a fixed Hg^{2+} concentration (20 ppb) in the presence of other metal ions (40 ppb) in 0.1 M AcB (pH 3.0). Mix indicates the solution containing Zn^{2+} , Cd^{2+} , Pb^{2+} , and Cu^{2+} (40 ppb) along with Hg^{2+} (20 ppb). The error bars represent the standard deviation for the mean of the three replicate tests.

3.6. Applications for Landfill Leachate Environment

To evaluate sensor behavior in a real wastewater matrix, landfill leachate samples were collected on site (Orange County Landfill, Orlando, FL, USA) without pretreatment except for filtration through 0.45 μm Polyethersulfone (PES) filters. The pH of the landfill leachate water was ~ 7.7 and included high heavy-metal and ionic concentration (Table S1). The pH was adjusted to 3.0 using 0.1 M HCl to have predominant species of Hg^{2+} in the range of pH 1–3 [53]. The original landfill leachate sample was directly used for the baseline curve and electrolyte due to a high NaCl concentration (13,800 $\mu\text{S}/\text{cm}$). Application of the AuNP-biopolymer-coated carbon SPE sensor in this experiment resulted in well-defined peaks at +0.6V for a range of Hg^{2+} concentrations, 0–100 ppb, for the landfill leachate, under which, the anodic peak potential shifted towards the positive due to the positive electrocatalytic activity of the Hg^{2+} ions with the sensor. This phenomenon is common as adsorption products tend to shift the peak potential positively [54]. Hg^{2+} sensitivity and the LOD of AuNP-biopolymer-coated carbon SPE sensor showed 0.089 $\mu\text{A}/\text{ppb}$ ($R^2 = 0.993$) and 1.69 ppb, respectively (Figure 8a,b). The reproducibility experiments conducted using landfill leachate spiked with Hg^{2+} (50 ppb) achieved 15 stable, successive measurements (Figure 8c) with an RSD of 5.1%. The concentrations of Hg^{2+} in the spiked landfill leachate sample were validated using ICP-MS and compared with the results of our method (Table 2). The recoveries were in the range of 98–108%, indicating an acceptable performance for practical applications.

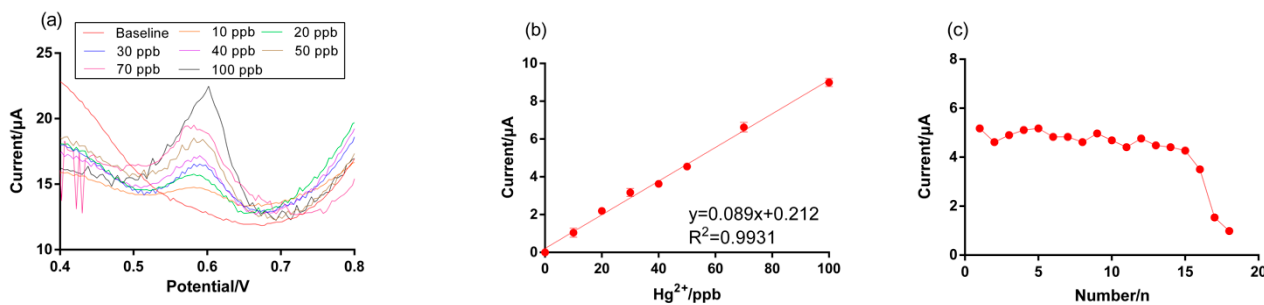


Figure 8. Hg^{2+} detection using a AuNP-biopolymer-coated carbon SPE sensor in a real landfill leachate environment (a) SWASV, (b) calibration curves, and (c) reproducibility (Hg^{2+} concentration is 50 ppb in landfill leachate (pH 3.0)). The error bars represent the standard deviation for the mean of the three replicate tests.

Table 2. Comparison of Hg²⁺ detection methods between AuNP-biopolymer-coated carbon SPE sensor and ICP-MS (n = 3).

| Sample | Hg ²⁺ Concentration | | | Recovery (%) |
|---------------------|--------------------------------|--|------------|--------------|
| | Add (ppb) | Detection (ppb) | | |
| | | AuNP-Biopolymer-Coated Carbon SPE Sensor | ICP-MS | |
| Landfill leachate 1 | 15 | 14.7 ± 1.8 | 15.2 ± 0.9 | 98 |
| Landfill leachate 2 | 20 | 21.6 ± 3.4 | 20.6 ± 1.3 | 107.8 |
| Landfill leachate 3 | 30 | 31.5 ± 2.1 | 30.8 ± 1.4 | 105 |

4. Conclusions

We demonstrated direct Hg²⁺ detection in landfill leachate using a newly developed AuNP-biopolymer carbon SPE sensor. The combination of the good conductivity of AuNP-chitosan and its strong adhesion to Hg²⁺ gave the sensor high sensitivity and selectivity for Hg²⁺ determination with a detection limit of 0.9 ppb in 0.1 M AcB. The sensor was successfully applied to determine Hg²⁺ in real landfill leachate samples directly with recovery ranging from 98 to 108%. The LOD and RSD for 15 consecutive measurements of the fabricated sensor in the landfill leachate samples were 1.69 ppb and 5.1%, respectively. The minimal interference in the presence of other heavy metal ions was observed in the detection of Hg²⁺ ions using the sensor. Overall, the developed AuNP-biopolymer carbon SPE sensor is expected to demonstrate reliable Hg²⁺ sensing in wastewater including landfill leachate.

Supplementary Materials: The following are available online at <https://www.mdpi.com/article/10.3390/mi12060649/s1>: Figure S1: Schematic of the AuNP-biopolymer-coated carbon SPE fabrication process; Figure S2: XPS and SEM-EDS spectra; Figure S3: Effect of deposition potential, deposition time, amplitude, and frequency on the anodic stripping peak current of Hg²⁺ using an AuNP-biopolymer-coated carbon SPE; Figure S4: SWASV and calibration curves of Hg²⁺ using different electrodes; Table S1: Heavy-metal ion concentrations in mining wastewater and soil leachate samples are shown in Table S1; Characterization of landfill leachate.

Author Contributions: J.-H.H. and W.H.L. conceived and designed the experiments. J.-H.H., D.F. and J.S. performed the experiments and analyzed the data. J.-H.H., D.F., J.S., V.A., L.Z. and W.H.L. wrote the manuscript. J.-H.H. and W.H.L. supervised the project. All authors discussed the results and contributed to the manuscript. All authors have read and agreed to the published version of the manuscript.

Funding: This work was supported by the Department of Energy (DOE) (Grant Number: DE-AC09-08SR22470) and the Korea Agency for Infrastructure Technology Advancement (KAIA) grant funded by the Ministry of Land, Infrastructure, and Transport (Grant Number: 21UGCP-B157945-02).

Conflicts of Interest: The authors declare no conflict of interest.

References

- Nolan, E.M.; Lippard, S.J. Tools and tactics for the optical detection of mercuric ion. *Chem. Rev.* **2008**, *108*, 3443–3480. [CrossRef]
- Chu, P.; Porcella, D. Mercury stack emissions from US electric utility power plants. *Water Air Soil Pollut.* **1995**, *80*, 135–144. [CrossRef]
- US EPA. *Mercury Update: Impact on Fish Advisories*; EPA-823-F-01-011; US EPA: Washington, DC, USA, 2001; pp. 1–10.
- Gworek, B.; Bemowska-Kalabun, O.; Kijeńska, M.; Wrzosek-Jakubowska, J. Mercury in marine and oceanic waters—A review. *Water Air Soil Pollut.* **2016**, *227*, 1–19. [CrossRef] [PubMed]
- Björkman, L.; Lundekvam, B.F.; Lægreid, T.; Bertelsen, B.I.; Morild, I.; Lilleng, P.; Lind, B.; Palm, B.; Vahter, M. Mercury in human brain, blood, muscle and toenails in relation to exposure: An autopsy study. *Environ. Health* **2007**, *6*, 1–14. [CrossRef] [PubMed]
- Ullrich, S.M.; Tanton, T.W.; Abdrashitova, S.A. Mercury in the aquatic environment: A review of factors affecting methylation. *Crit. Rev. Environ. Sci. Technol.* **2001**, *31*, 241–293. [CrossRef]

7. Tchounwou, P.B.; Yedjou, C.G.; Patlolla, A.K.; Sutton, D.J. Heavy metal toxicity and the environment. *Mol. Clin. Environ. Toxicol.* **2012**, *101*, 133–164.
8. Hoang, C.V.; Oyama, M.; Saito, O.; Aono, M.; Nagao, T. Monitoring the presence of ionic mercury in environmental water by plasmon-enhanced infrared spectroscopy. *Sci. Rep.* **2013**, *3*, 1–6. [[CrossRef](#)] [[PubMed](#)]
9. Davidson, P.W.; Myers, G.J.; Weiss, B. Mercury exposure and child development outcomes. *Pediatrics* **2004**, *113*, 1023–1029.
10. Weinstein, M.; Bernstein, S. Pink ladies: Mercury poisoning in twin girls. *Cmaj* **2003**, *168*, 201.
11. Genchi, G.; Sinicropi, M.S.; Carocci, A.; Lauria, G.; Catalano, A. Mercury exposure and heart diseases. *Int. J. Environ. Res. Public Health* **2017**, *14*, 74. [[CrossRef](#)]
12. Fernandes Azevedo, B.; Barros Furieri, L.; Peçanha, F.M.; Wiggers, G.A.; Frizera Vassallo, P.; Ronacher Simões, M.; Fiorim, J.; Rossi de Batista, P.; Fioresi, M.; Rossoni, L. Toxic effects of mercury on the cardiovascular and central nervous systems. *J. Biomed. Biotechnol. Bioeng.* **2012**, *2012*. [[CrossRef](#)] [[PubMed](#)]
13. Alves, G.M.; Magalhães, J.M.; Soares, H.M. Voltammetric quantification of Zn and Cu, together with Hg and Pb, based on a gold microwire electrode, in a wider spectrum of surface waters. *Electroanalysis* **2013**, *25*, 493–502. [[CrossRef](#)]
14. Sanchez-Rodas, D.; Corns, W.; Chen, B.; Stockwell, P. Atomic fluorescence spectrometry: A suitable detection technique in speciation studies for arsenic, selenium, antimony and mercury. *J. Anal. At. Spectrom.* **2010**, *25*, 933–946. [[CrossRef](#)]
15. Passariello, B.; Barbaro, M.; Quaresima, S.; Casciello, A.; Marabini, A. Determination of mercury by inductively coupled plasma—Mass spectrometry. *Microchem. J.* **1996**, *54*, 348–354. [[CrossRef](#)]
16. Margui, E.; Kregsamer, P.; Hidalgo, M.; Tapias, J.; Queral, I.; Strel, C. Analytical approaches for Hg determination in wastewater samples by means of total reflection X-ray fluorescence spectrometry. *Talanta* **2010**, *82*, 821–827. [[CrossRef](#)]
17. Leopold, K.; Harwardt, L.; Schuster, M.; Schlemmer, G. A new fully automated on-line digestion system for ultra trace analysis of mercury in natural waters by means of FI-CV-AFS. *Talanta* **2008**, *76*, 382–388. [[CrossRef](#)]
18. Pyhtilä, H.; Perämäki, P.; Piispanen, J.; Niemelä, M.; Suoranta, T.; Starr, M.; Nieminen, T.; Kantola, M.; Ukonmaanaho, L. Development and optimization of a method for detecting low mercury concentrations in humic-rich natural water samples using a CV-ICP-MS technique. *Microchem. J.* **2012**, *103*, 165–169. [[CrossRef](#)]
19. Wei, Y.; Yang, R.; Yu, X.-Y.; Wang, L.; Liu, J.-H.; Huang, X.-J. Stripping voltammetry study of ultra-trace toxic metal ions on highly selectively adsorptive porous magnesium oxide nanoflowers. *Analyst* **2012**, *137*, 2183–2191. [[CrossRef](#)] [[PubMed](#)]
20. Zaib, M.; Athar, M.M.; Saeed, A.; Farooq, U. Electrochemical determination of inorganic mercury and arsenic—A review. *Biosens. Bioelectron.* **2015**, *74*, 895–908. [[CrossRef](#)]
21. Huber, J.; Leopold, K. Nanomaterial-based strategies for enhanced mercury trace analysis in environmental and drinking waters. *TrAC Trends Anal. Chem.* **2016**, *80*, 280–292. [[CrossRef](#)]
22. Gao, C.; Huang, X.-J. Voltammetric determination of mercury (II). *TrAC Trends Anal. Chem.* **2013**, *51*, 1–12. [[CrossRef](#)]
23. Tung, T.T.; Nine, M.J.; Krebsz, M.; Pasinszki, T.; Coghlan, C.J.; Tran, D.N.; Losic, D. Recent advances in sensing applications of graphene assemblies and their composites. *Adv. Funct. Mater.* **2017**, *27*, 1702891. [[CrossRef](#)]
24. Lin, Y.; Peng, Y.; Di, J. Electrochemical detection of Hg (II) ions based on nanoporous gold nanoparticles modified indium tin oxide electrode. *Sens. Actuators B Chem.* **2015**, *220*, 1086–1090. [[CrossRef](#)]
25. Fu, X.-C.; Wu, J.; Nie, L.; Xie, C.-G.; Liu, J.-H.; Huang, X.-J. Electropolymerized surface ion imprinting films on a gold nanoparticles/single-wall carbon nanotube nanohybrids modified glassy carbon electrode for electrochemical detection of trace mercury (II) in water. *Anal. Chim. Acta* **2012**, *720*, 29–37. [[CrossRef](#)] [[PubMed](#)]
26. Lu, X.; Dong, X.; Zhang, K.; Zhang, Y. An ultrasensitive electrochemical mercury (II) ion biosensor based on a glassy carbon electrode modified with multi-walled carbon nanotubes and gold nanoparticles. *Anal. Methods* **2012**, *4*, 3326–3331. [[CrossRef](#)]
27. Somé, I.T.; Sakira, A.K.; Mertens, D.; Ronkart, S.N.; Kauffmann, J.-M. Determination of groundwater mercury (II) content using a disposable gold modified screen printed carbon electrode. *Talanta* **2016**, *152*, 335–340. [[CrossRef](#)] [[PubMed](#)]
28. Takale, B.S.; Bao, M.; Yamamoto, Y. Gold nanoparticle (AuNPs) and gold nanopore (AuNPore) catalysts in organic synthesis. *Org. Biomol. Chem.* **2014**, *12*, 2005–2027. [[CrossRef](#)]
29. Hezard, T.; Fajerweg, K.; Evrard, D.; Collière, V.; Behra, P.; Gros, P. Gold nanoparticles electrodeposited on glassy carbon using cyclic voltammetry: Application to Hg (II) trace analysis. *J. Electroanal. Chem.* **2012**, *664*, 46–52. [[CrossRef](#)]
30. Zanini, V.I.P.; Gimenez, R.E.; Pérez, O.E.L.; de Mishima, B.A.L.; Borsarelli, C.D. Enhancement of amperometric response to tryptophan by proton relay effect of chitosan adsorbed on glassy carbon electrode. *Sens. Actuators B Chem.* **2015**, *209*, 391–398. [[CrossRef](#)]
31. Luo, X.; Zeng, J.; Liu, S.; Zhang, L. An effective and recyclable adsorbent for the removal of heavy metal ions from aqueous system: Magnetic chitosan/cellulose microspheres. *Bioresour. Technol.* **2015**, *194*, 403–406. [[CrossRef](#)]
32. Ghalkhani, M.; Shahrokhian, S. Adsorptive stripping differential pulse voltammetric determination of mebendazole at a graphene nanosheets and carbon nanospheres/chitosan modified glassy carbon electrode. *Sens. Actuators B Chem.* **2013**, *185*, 669–674. [[CrossRef](#)]
33. Amanulla, B.; Subbu, H.K.R.; Ramaraj, S.K. A sonochemical synthesis of cyclodextrin functionalized Au-FeNPs for colorimetric detection of Cr⁶⁺ in different industrial waste water. *Ultrason. Sonochem.* **2018**, *42*, 747–753. [[CrossRef](#)]
34. Hwang, J.-H.; Wang, X.; Pathak, P.; Rex, M.M.; Cho, H.J.; Lee, W.H. Enhanced electrochemical detection of multiheavy metal ions using a biopolymer-coated planar carbon electrode. *IEEE Trans. Instrum. Meas.* **2019**, *68*, 2387–2393. [[CrossRef](#)]

35. Lee, W.H.; Wahman, D.G.; Pressman, J.G. Amperometric carbon fiber nitrite microsensor for in situ biofilm monitoring. *Sens. Actuators B Chem.* **2013**, *188*, 1263–1269. [[CrossRef](#)]
36. Quan, Z.; Wang, Y.; Fang, J. High-Index Faceted Noble Metal Nanocrystals. *Acc. Chem. Res.* **2013**, *46*, 191–202. [[CrossRef](#)] [[PubMed](#)]
37. Yuanfeng, P.; Ruiyi, L.; Xiulan, S.; Guangli, W.; Zaijun, L. Highly sensitive electrochemical detection of circulating tumor DNA in human blood based on urchin-like gold nanocrystal-multiple graphene aerogel and target DNA-induced recycling double amplification strategy. *Anal. Chim. Acta* **2020**, *1121*, 17–25. [[CrossRef](#)] [[PubMed](#)]
38. Van Santen, R.A. Complementary Structure Sensitive and Insensitive Catalytic Relationships. *Acc. Chem. Res.* **2009**, *42*, 57–66. [[CrossRef](#)] [[PubMed](#)]
39. Alegria, E.C.B.A.; Ribeiro, A.P.C.; Mendes, M.; Ferraria, A.M.; Do Rego, A.M.B.; Pombeiro, A.J.L. Effect of Phenolic Compounds on the Synthesis of Gold Nanoparticles and its Catalytic Activity in the Reduction of Nitro Compounds. *Nanomaterials* **2018**, *8*, 320. [[CrossRef](#)]
40. Tang, L.; Feng, H.; Cheng, J.; Li, J. Uniform and rich-wrinkled electrophoretic deposited graphene film: A robust electrochemical platform for TNT sensing. *Chem. Commun.* **2010**, *46*, 5882–5884. [[CrossRef](#)] [[PubMed](#)]
41. Gong, J.; Zhou, T.; Song, D.; Zhang, L. Monodispersed Au nanoparticles decorated graphene as an enhanced sensing platform for ultrasensitive stripping voltammetric detection of mercury (II). *Sens. Actuators B Chem.* **2010**, *150*, 491–497. [[CrossRef](#)]
42. Kang, W.; Pei, X.; Rusinek, C.A.; Bange, A.; Haynes, E.N.; Heineman, W.R.; Papautsky, I. Determination of lead with a copper-based electrochemical sensor. *Anal. Chem.* **2017**, *89*, 3345–3352. [[CrossRef](#)] [[PubMed](#)]
43. Rahman, M.T.; Kabir, M.F.; Gurung, A.; Reza, K.M.; Pathak, R.; Ghimire, N.; Baride, A.; Wang, Z.; Kumar, M.; Qiao, Q. Graphene oxide–silver nanowire nanocomposites for enhanced sensing of Hg²⁺. *ACS Appl. Nano Mater.* **2019**, *2*, 4842–4851. [[CrossRef](#)]
44. Wei, Y.; Yang, R.; Liu, J.-H.; Huang, X.-J. Selective detection toward Hg (II) and Pb (II) using polypyrrole/carbonaceous nanospheres modified screen-printed electrode. *Electrochim. Acta* **2013**, *105*, 218–223. [[CrossRef](#)]
45. Koper, N.; Leston, L.; Baker, T.M.; Curry, C.; Rosa, P. Effects of ambient noise on detectability and localization of avian songs and tones by observers in grasslands. *Ecol. Evol.* **2016**, *6*, 245–255. [[CrossRef](#)]
46. Rex, M.; Hernandez, F.E.; Campiglia, A.D. Pushing the limits of mercury sensors with gold nanorods. *Anal. Chem.* **2006**, *78*, 445–451. [[CrossRef](#)]
47. Li, D.; Li, J.; Jia, X.; Wang, E. Gold nanoparticles decorated carbon fiber mat as a novel sensing platform for sensitive detection of Hg (II). *Electrochem. Commun.* **2014**, *42*, 30–33. [[CrossRef](#)]
48. Matlou, G.G.; Nkosi, D.; Pillay, K.; Arotiba, O. Electrochemical detection of Hg (II) in water using self-assembled single walled carbon nanotube-poly (m-amino benzene sulfonic acid) on gold electrode. *Sens. Biosens. Res.* **2016**, *10*, 27–33. [[CrossRef](#)]
49. Wei, J.; Yang, D.; Chen, H.; Gao, Y.; Li, H. Stripping voltammetric determination of mercury (II) based on SWCNT-PhSH modified gold electrode. *Sens. Actuators B Chem.* **2014**, *190*, 968–974. [[CrossRef](#)]
50. Bernalte, E.; Sánchez, C.M.; Gil, E.P. Determination of mercury in ambient water samples by anodic stripping voltammetry on screen-printed gold electrodes. *Anal. Chim. Acta* **2011**, *689*, 60–64. [[CrossRef](#)]
51. Safavi, A.; Farjami, E. Construction of a carbon nanocomposite electrode based on amino acids functionalized gold nanoparticles for trace electrochemical detection of mercury. *Anal. Chim. Acta* **2011**, *688*, 43–48. [[CrossRef](#)]
52. Punrat, E.; Chuanuwatanakul, S.; Kaneta, T.; Motomizu, S.; Chailapakul, O. Method development for the determination of mercury (II) by sequential injection/anodic stripping voltammetry using an in situ gold-film screen-printed carbon electrode. *J. Electroanal. Chem.* **2014**, *727*, 78–83. [[CrossRef](#)]
53. Alguacil, F.J.; López, F.A. Adsorption Processing for the Removal of Toxic Hg (II) from Liquid Effluents: Advances in the 2019 Year. *Metals* **2020**, *10*, 412. [[CrossRef](#)]
54. Gao, W.; Nyein, H.Y.; Shahpar, Z.; Fahad, H.M.; Chen, K.; Emaminejad, S.; Gao, Y.; Tai, L.-C.; Ota, H.; Wu, E. Wearable microsensor array for multiplexed heavy metal monitoring of body fluids. *ACS Sens.* **2016**, *1*, 866–874. [[CrossRef](#)]